(Received 6 December 2024, Accepted 13 March 2025, Scheduled 28 March 2025)

A Novel Asymmetric Spoof Surface Plasmon Polariton Transmission Line for High Gain Endfire Radiation Using Phase Reversal Condition

Dhruba C. Panda[1,*], Bikash K. Santi[1], Biku Raut[1], Deepak K. Naik[1], and Rajanikanta Swain[2]

[1]*Department of Electronic Science, Berhampur University, Berhampur 760007, Odisha, India*
[2]*Electronics Center of Excellence, Bhubaneswar 751024, Odisha, India*

ABSTRACT: This paper introduces a novel asymmetric design for spoof surface plasmon polariton (SSPP) transmission line-based endfire antenna. It utilizes the phase reversal condition in an asymmetric SSPP transmission line to achieve high gain endfire radiation. The antenna design uses mono-planar fabrication using the CPW concept. Achieving asymmetry in the SSPP transmission line involves simply bending a straight SSPP transmission line containing H-shaped unit cells. Successive upward and downward bending of the transmission line introduces the phase reversal condition and increases the antenna's gain. Notably, there are no limitations on the length over which bending occurs to achieve the phase reversal condition. Simple design principles, a single-layer configuration, and high gain are the advantages of the antenna. Results from the fabricated prototype closely match simulation results. Within the 7.7–8.3 GHz operating band, the antenna exhibits a 7.5% bandwidth and a peak gain of 13.6 dBi. It can find applications in various wireless communication systems requiring high gain and endfire radiations.

1. INTRODUCTION

Planar high gain endfire antennas are attracting attention in various airborne applications, buried object detection, microwave imaging, and vehicular communications. Currently, they mostly include Yagi-Uda [1] and substrate integrated waveguide (SIW) based planar antennas [2]. However, these antennas face limitations in achieving high gain at high frequencies. A technique to improve gain and efficiency is the minimisation of ohmic losses by reduction/removal of the ground plane. In the microwave domain, spoof surface plasmon polariton (SSPP) transmission line is a new concept proposed at the beginning of this century [3]. It consists of sub-wavelength unilateral or bilateral corrugations on planar transmission lines, offering advantages such as low loss, large field confinement, and light weight [4]. As it reduces ohmic loss, researchers are actively trying to employ it in the design of endfire antennas with higher gain. These antennas are suitable for microwave, mmwave, and terahertz frequencies [5–8]. Besides, SSPP also finds applications in sensor design [9, 10].

SSPP-based endfire antennas, specifically single-layer structures, offer better accommodation than double-layer structures in wireless communication systems. Asymmetry is the key requirement to achieve endfire radiation in an SSPP transmission line. The authors in [11] propose a unilateral corrugated SSPP single-layer endfire antenna. It gives a maximum gain of 9.2 dBi within the frequency range of 7.5 to 8.5 GHz. Ge et al. [12] use the Goubau line concept [13] and Hansan-Wood condition [14] in a bilateral asymmetrical SSPP transmission line to design endfire antenna. The antenna provides an average gain of 9.9 dBi within the operating band 13–15 GHz. Similarly, in [15], the authors use an asymmetric SSPP line with an elliptical director to achieve near-endfire radiation. This design exhibits a gain of 10.5 to 12.1 dBi within the operating frequency 15.75–17.5 GHz.

Recent studies use phase reversal techniques within asymmetrical structures to generate endfire radiation [16]. Utilizing this concept, one approach [17] uses sections with sinusoidal bulged-out unit cells to introduce asymmetry and increase the gain. Another approach [18] involves producing asymmetry by altering groove depth inside an H-type unit cell in a section. Three such sections are combined to achieve high gain. The sectional length determination for phase reversal includes a parametric study [17] and an effective array factor [18]. However, there is neither a closed-form formula for sectional length nor an alternative technique.

This paper proposes a novel asymmetric single-layer SSPP transmission line-based antenna to achieve high gain endfire radiation. The SSPP transmission line uses H-shaped unit cells. Bending the transmission line introduces asymmetry naturally, and subsequent bending in the opposite direction automatically introduces phase reversal. Therefore, determining the sectional length where phase reversal occurs is not required.

The remaining parts of this paper follow the following organization. Section 2 outlines the evolution of the asymmetric SSPP transmission line, analyzes unit cells, describes the antenna, and explains its operating principle. Section 3 conducts a parametric study of the antenna. Section 4 presents the results

* Corresponding author: Dhruba Charan Panda (dcpanda@gmail.com).

and discussion of the fabricated prototype. Finally, Section 5 presents the conclusion derived.

2. ANTENNA DESCRIPTION

2.1. Asymmetric SSPP Transmission Line Evolution

Asymmetry in a corrugated SSPP transmission line is essential for supporting two different modes, which stops the cancellation of the net transverse electric field in the endfire direction. Typically, the design of an asymmetric transmission line involves the periodic joining of unit cells with different groove depths. An asymmetric transmission line supports a dipole moment wave resulting from the two modes, which is responsible for endfire radiation in the transmission line segment. The generation of the two modes stems from the nonuniform charge distribution in an asymmetric unit cell. When such an asymmetric section, along with its inverted counterpart, is cascaded, it results in a high gain endfire antenna. However, the electric field should undergo a phase reversal at the junction. In an asymmetric SSPP antenna, the phase difference between the modes gradually increases from zero to π. As a result, the coupling between the two modes gradually decreases to zero. Therefore, a phase reversal at this point is required to start the coupling between the two modes. In addition, there is a trade-off between cross-aperture and endfire gain. Phase reversal has been proven to break this trade-off. Consequently, an SSPP antenna with a small cross aperture can give a larger gain.

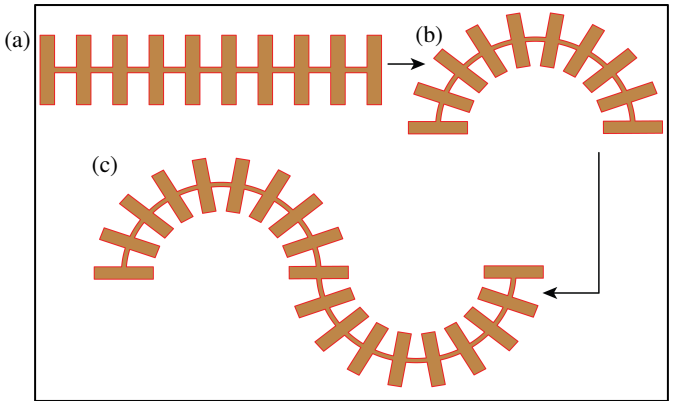

FIGURE 1. Antenna evolution (a) Symmetric Straight SSPP TL with uniform H unit cells, (b) Bent asymmetric SSPP TL segment with asymmetric unit cells, and (c) Combined inverted segments.

Figure 1 shows the proposed evolution of the asymmetric SSPP transmission line. The evolution starts with an SSPP line comprising uniform H-shaped unit cells (Fig. 1(a)), known for their ease of design. As the transmission line is bent upward, H cells have more flaring on the top and less flaring towards the bottom (Fig. 1(b)). This simple bending makes the SSPP line asymmetric. Subsequently, the line is bent downward, resulting in a section with unit cells having more flaring towards the bottom and less flaring towards the top. These two bendings are akin to joining an asymmetric SSPP transmission line section with its inverted counterpart (Fig. 1(c)). This iterative process continues until the gain saturates. The junction of the sections marks the point where phase reversal occurs.

2.2. Unit Cell Analysis

To analyze the dispersion characteristics of the unit cell with respect to its geometrical parameters, we conduct an eigenmode analysis of the unit cell using HFSS. Fig. 2 illustrates the geometrical parameters of both unmodified and modified cells in insets (a) and (b), respectively. We vary the degree of asymmetry in the cells by adjusting 'l' while keeping 'a' fixed. The dispersion curves lie between the curves of the light line and the unmodified H-shaped unit cell. As the flaring decreases with decreasing l, the curve approaches the light line. Conversely, increasing the flaring by increasing l causes the curve to approach the curve of the unmodified cell. Fig. 3 displays the two eigenmodes of the modified unit cell, existing within the frequencies 7.7 and 8.3 GHz. Due to the difference in charge distribution, the structure supports two modes. Mode 1 is due to the wider part of the H-shaped cell and mode 2 due to the narrow part of the cell. Table 1 provides the values of the considered unit cell for the antenna design.

TABLE 1. Physical parameters of the unit cell (Unit: mm).

s	p_e	l	h	a
8.7	7	3	4	1.5

2.3. Proposed Antenna

Figure 4 depicts schematics of the antenna, consisting of a coplanar waveguide (CPW) feed section, CPW to SSPP transition section, antenna section, and tapered termination section. The antenna section incorporates seven asymmetric bent sections. To achieve a smooth transition from the CPW to SSPP mode, we incorporated a tapered section and gradually increased the height of the H-shaped unit cells. The CPW transmission line was designed to maintain a 50 Ω characteristic impedance. We employed a flared CPW using the function $y = f(x) = e^{\gamma x} - 1$ as an impedance transformer, as the SSPP line operates as a high-impedance transmission line. Here, $\gamma = \ln(w/2 - h_1/2 - h_c + 1) \,/\, l_t$. A matched tapered section terminates the antenna to release the radiative fields. Table 2 gives the antenna dimensions.

TABLE 2. Physical parameters of the antenna (Unit: mm).

L	W	l_c	l_t	d
332	70	10	47.5	28
h_c	g_t	l_1	l_2	h_1
0.2	4	12	30	2.3

2.4. Phase Reversal Analysis

Consider p as the dipole moment density resulting from the asymmetric charge distribution ρ_1 and ρ_2 in an asymmetric unit cell. Let's assume that p forms an angle α with the x-axis (see Fig. 4). Consequently, p has two components: $p_x = p\cos\alpha$

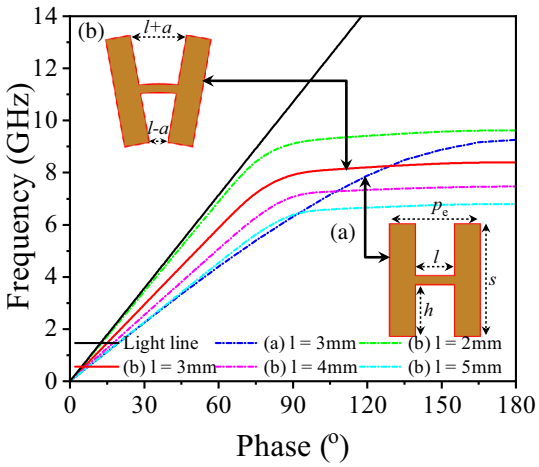

FIGURE 2. Dispersion curves. (a) Unmodified unit cell and (b) modified unit cell.

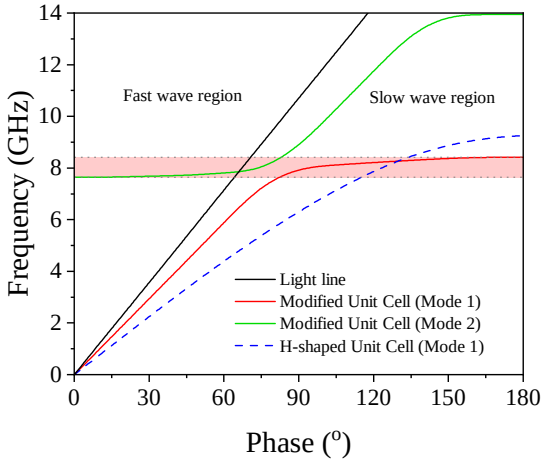

FIGURE 3. Dispersion curves of two modes of modified unit cell.

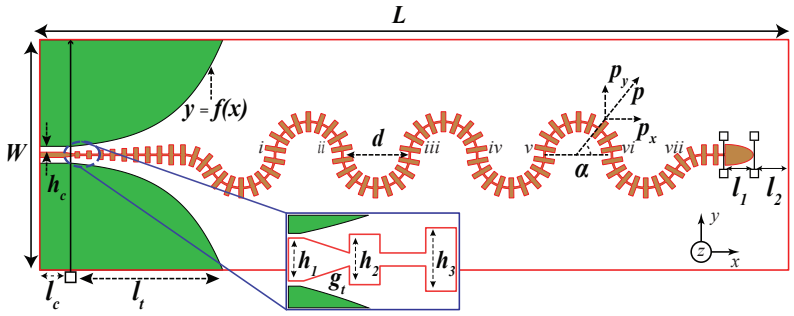

FIGURE 4. Geometry of the proposed antenna showing the front view.

and $p_y = p\sin\alpha$. The equal and opposite p_x components over a segment cancel each other. As a result, p_y component only contributes to the two travelling modes along the x-axis from the asymmetric charge distribution on a segment. Let β_1 and β_2 be their respective propagation constants. The traveling waves due to β_1 and β_2 can be written as $\rho_1 = \rho_o e^{j\beta_1 x}$ and $\rho_2 = \rho_o e^{j\beta_2 x}$.

Therefore, the dipole moment wave p_y, due to ρ_1 and ρ_2, can now be written as:

$$p_y = p\sin\alpha \propto \rho_1 - \rho_2 = -j2\rho_0 \sin(\Delta\beta x)e^{-j(\bar{\beta}x)}dx \quad (1)$$

where $\Delta\beta = (\beta_1 - \beta_2)/2$ and $\overline{\beta} = (\beta_1 + \beta_2)/2$.

Now,

$$|E_{endfire}| \propto \left| \int_0^l p_y dx \right| \quad (2)$$

Since α is 0 at one end and 180 degrees at the other, the fields undergo a phase reversal at the ends of a segment. The fields along the x-axis are depicted in Fig. 5, where peaks [12] are observed at points i, ii, …, vii (Fig. 4), confirming phase reversals at the junctions. Therefore, we have the freedom to choose the length of the segment, which is a distinctive advantage of the present design method over methods [12] and [18].

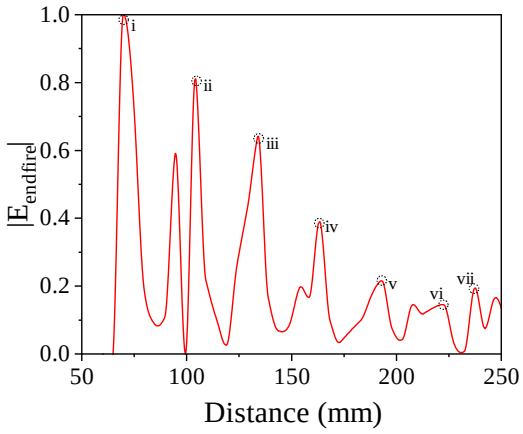

FIGURE 5. Normalized field intensity versus length at 8 GHz.

3. PARAMETRIC STUDY OF THE ANTENNA

Figure 5 indicates that the fields do not completely decay to zero down the segments. To increase the antenna's gain, it is feasible to include additional segments. Thus, the number of segments determines the antenna's gain. Additionally, the number of cells per segment regulates the strength of the dipole wave. In this section, we present the simulation studies of the gain performance of the antenna based on these two parameters.

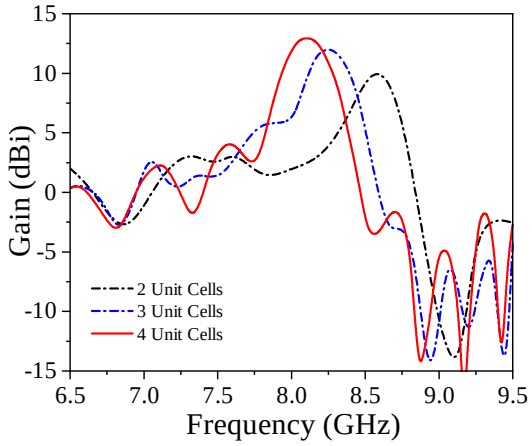

FIGURE 6. Simulated gain vs number of unit cells per segment.

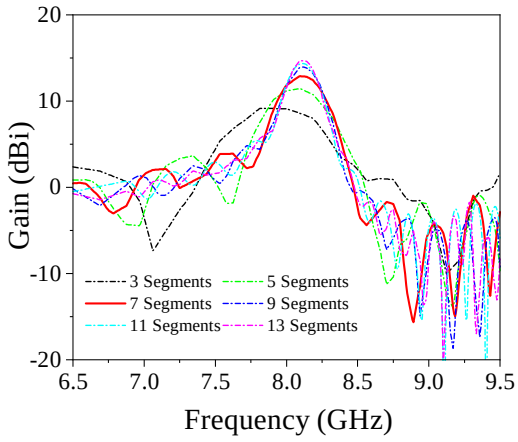

FIGURE 7. Simulated gain vs number of segments.

TABLE 3. Performance comparison with other reported works.

Ref.	f	Gain (dBi)	BW (%)	Length (λ_0)	Radiating length (λ_0)	Height (λ_0)	Efficiency (%)
[12]	13–15	8.56–10.7	14	4.67	1.26	0.03	82
[15]	15.75–17.5	10.5–12.1	11	5.8	2	0.055	95
[17]	5.25–7.94	7.2–11.7	40.8	4	1.54	0.011	-
[18]	17–19	12.9–16.2	11	7.8	3.6	0.03	87
Ours	7.7–8.3	12–13.6	7.5	8.85	5.22	0.013	95

3.1. Gain vs Number of Unit Cells Per Segment

Figure 6 depicts the simulated gain versus the number of unit cells per segment. We conducted simulations while keeping the number of segments constant at 7. As the cells per segment increase from 2 to 4, the peak gain initially rises rapidly before reaching saturation. Additionally, the peak gain shifts towards the lower frequency and stabilizes at 8 GHz. Any further enhancement in gain is not achievable due to reaching the phase reversal condition.

3.2. Gain vs Number of Segments

Figure 7 illustrates the variation in gain with respect to the number of segments. Initially, as the number of segments increases, the peak gain increases. However, with further increases in the number of segments, the peak gain augmentation slows down, converging at approximately 8 GHz. Any further increase in peak gain becomes unattainable as all incident energies are effectively radiated out. Therefore, we consider the antenna with 7 segments as the optimal configuration.

TABLE 4. Beam width comparison.

[12]	13 GHz	14 GHz	15 GHz
XY Plane	$\sim 30^\circ$	~ 30	$\sim 35^\circ$
XZ Plane	$\sim 30^\circ$	$\sim 20^\circ$	$\sim 30^\circ$
[15]	16.5 GHz	17 GHz	17.5 GHz
XY Plane	$\sim 20^\circ$	$\sim 20^\circ$	$\sim 15^\circ$
XZ Plane	$\sim 60^\circ$	$\sim 60^\circ$	$\sim 50^\circ$
[17]	5.3 GHz	7.1 GHz	7.9 GHz
XY Plane	$\sim 30^\circ$	$\sim 20^\circ$	$\sim 15^\circ$
XZ Plane	$\sim 30^\circ$	$\sim 45^\circ$	$\sim 20^\circ$
[18]	17 GHz	18 GHz	19 GHz
XY Plane	$\sim 45^\circ$	$\sim 30^\circ$	$\sim 30^\circ$
XZ Plane	$\sim 30^\circ$	$\sim 30^\circ$	$\sim 35^\circ$
Our Work	8.1 GHz	8.2 GHz	8.3 GHz
XY Plane	50°	30°	15°
XZ Plane	20°	15°	10°

4. RESULTS AND DISCUSSIONS

We selected unit cell dimensions (Table 1) that offer optimal performance at 8 GHz to design the antenna (Table 2). Additionally, we chose 4 unit cells per segment and 7 segments. After finalizing the dimensions, we employed HFSS to simulate the antenna. Fig. 9 shows a snapshot of the electric field in the endfire direction at 8 GHz. It indicates the radiation of fields in the endfire direction. We fabricated a prototype to validate the simulation results, using a Pegaclad 300 substrate with a dielectric constant of 3.0 and a loss tangent of 0.002. Fig. 10 depicts a snapshot of the fabricated prototype. The S_{11} and gain plots of the simulated and measured results are presented in Figs. 11 and 12, respectively. Fig. 11 indicates that the magnitude of S_{11} remains below -10 dB in the operating frequency region, suggesting good impedance matching. Similarly, Fig. 12 illustrates that the antenna's gain lies between 12 and 13.6 dBi

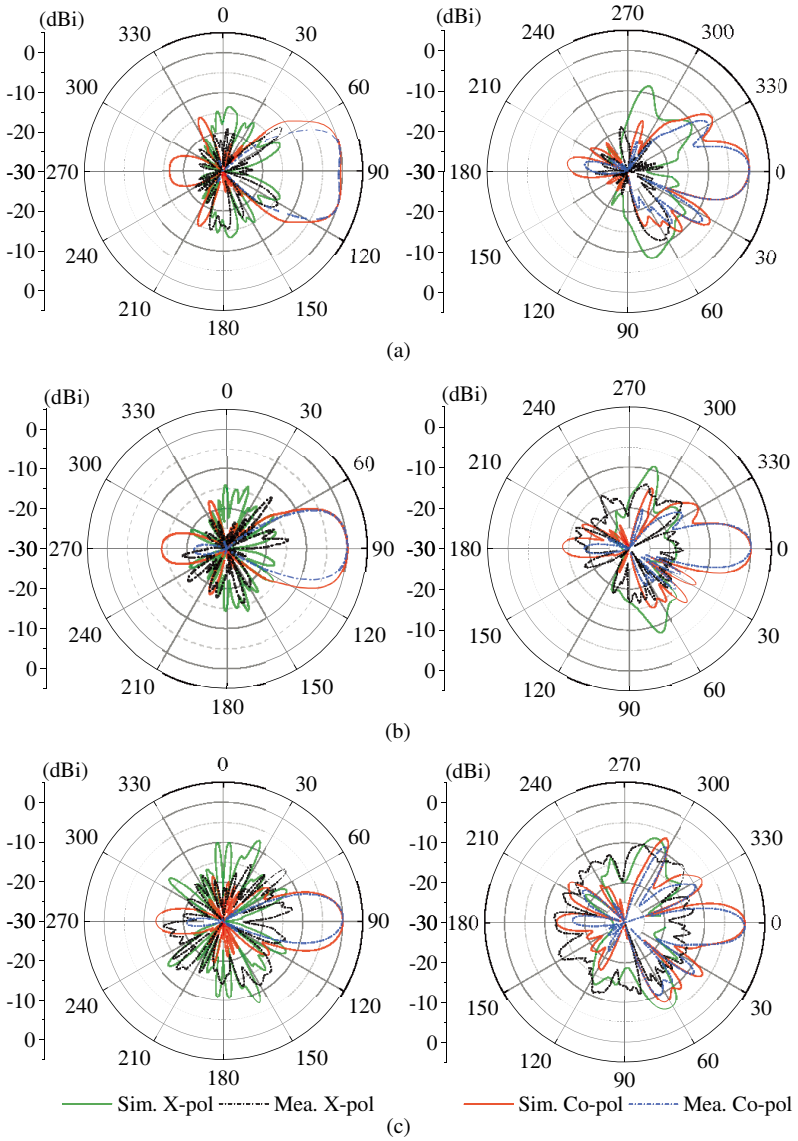

FIGURE 8. Simulated and measured normalized radiation patterns with co-and cross-polarization in xy and xz planes: (a) 8.1 GHz, (b) 8.2 GHz, and (c) 8.3 GHz.

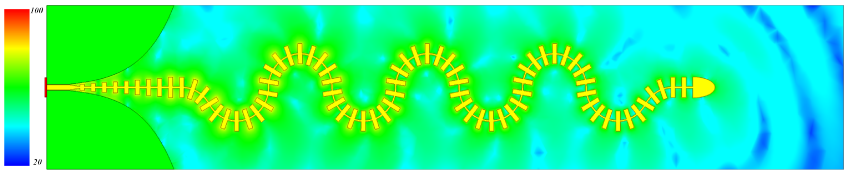

FIGURE 9. Simulated E-field at 8 GHz.

within the desired frequency band. Additionally, the antenna demonstrates an efficiency around 95%. Radiation patterns of the antenna at 8.1, 8.2, and 8.3 GHz are given in Fig. 8 showing endfire radiation. It shows that the simulated patterns closely follow the measured ones.

To compare our antenna's performance, we consider recently reported single-layer SSPP-based endfire antennas. We analyze the gain, bandwidth, substrate thickness, and radiation efficiency of the antennas. Table 3 gives the comparisons. Antenna [15] utilizes an additional elliptical director to generate endfire radiation but lacks generalization in the design procedure. Conversely, in the case of antenna [17], which employs asymmetry and phase reversal, minor pattern variations are observed towards the endfire direction. The comparison among [12, 18], and our antenna is based on clear design guidelines focusing on asymmetry and phase reversal. Our present antenna exhibits nearly identical performance in terms of gain and bandwidth compared to antenna [18]. Table 4 compares the

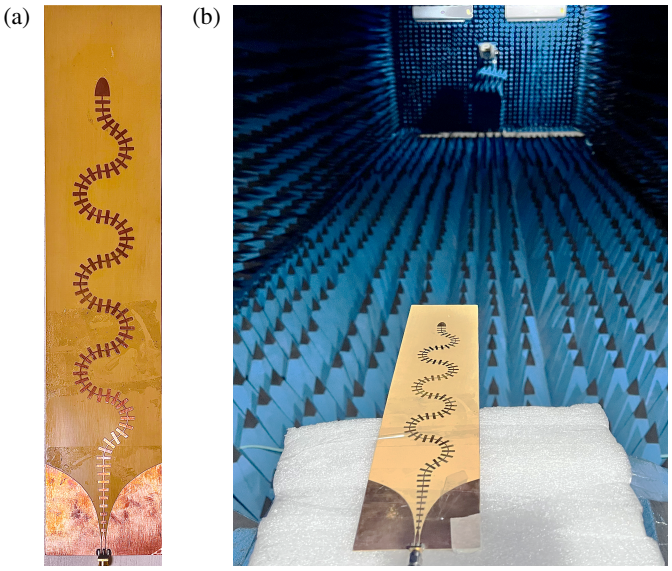

FIGURE 10. (a) Fabricated prototype. (b) Setup inside anechoic chamber.

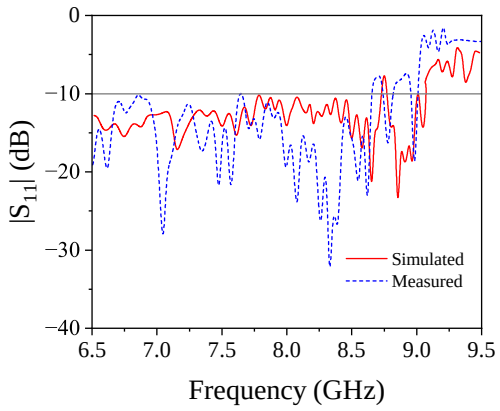

FIGURE 11. Simulated and measured reflection responses.

3-dB beamwidth of the antennas. It can be seen that the proposed antenna shows minimum beamwidth in the XZ plane. Overall, our antenna is the simplest to design, has low profile, demonstrates stable high gain, and possesses high radiation efficiency.

5. CONCLUSION

This paper proposes a new endfire antenna design using an asymmetric SSPP transmission line. The asymmetry is achieved by simply bending an SSPP straight transmission line. To achieve phase reversal, the design incorporates continuous up and down bends. This approach results in a high gain endfire antenna with stable radiation patterns. The proposed antenna offers several advantages: low profile, high gain, single layer, and simple design procedure. The simulated results for a prototype antenna show good agreement with the measured ones. Due to its high gain and low-profile design, the antenna is well suited for microwave imaging in lossy media, radar systems, and high-data-rate point-to-point wireless communication applications.

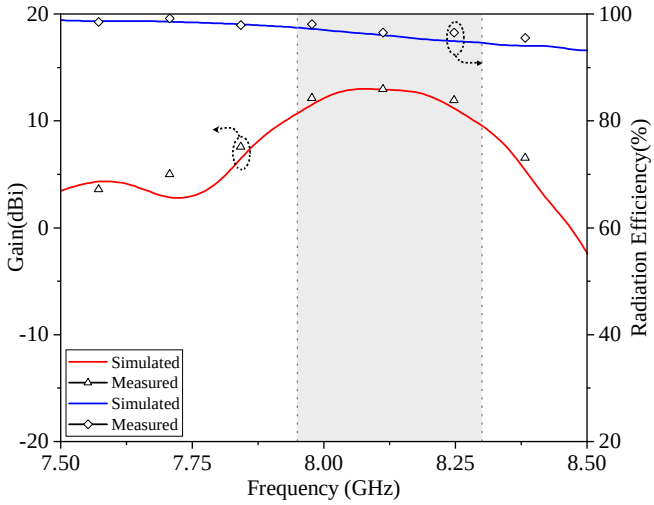

FIGURE 12. Simulated and measured gains.

ACKNOWLEDGEMENT

Financial support provided by SERB, DST, Govt. of India under grant No. CRG/2023/007781 to D. C. Panda is gratefully acknowledged.

REFERENCES

[1] Chopra, R. and G. Kumar, "Compact, broadband, and high gain directional endfire antenna," *Microwave and Optical Technology Letters*, Vol. 62, No. 7, 2546–2553, 2020.

[2] Tian, Y. Z., Y. M. Pan, X. Y. Liu, and K. W. Leung, "An SIW-based wideband endfire filtering magneto-electric dipole antenna for millimeter-wave applications," *IEEE Transactions on Antennas and Propagation*, Vol. 71, No. 12, 9986–9991, 2023.

[3] Pendry, J. B., L. Martin-Moreno, and F. J. Garcia-Vidal, "Mimicking surface plasmons with structured surfaces," *Science*, Vol. 305, No. 5685, 847–848, 2004.

[4] Chaparala, R., S. Imamvali, and S. Tupakula, "Enhancement of spoof surface plasmon polariton waveguide performance through modified groove width," *Optical Engineering*, Vol. 63, No. 5, 055102, 2024.

[5] Xiao, B., X. Tu, A. Fyffe, X. Wang, and Z. Shi, "A compact, high gain, spoof surface plasmon polariton sawtooth end-fire antenna," *Journal of Modern Optics*, Vol. 67, No. 7, 654–660, 2020.

[6] Li, W. and W. Zhao, "Miniaturized low-profile end-fire antenna based on spoof surface plasmon polaritons," *Applied Physics A*, Vol. 130, No. 11, 796, Oct. 2024.

[7] Bao, Y., Y.-B. Wang, T.-H. Zhang, and L.-Y. Zhao, "A novel ultra-wideband end-fire antenna based on spoof surface plasma polaritons," *Frequenz*, Vol. 79, No. 1-2, 71–80, 2025.

[8] Zhao, H., J. Li, Q. Zhang, S. Li, and X. Yin, "Spoof surface plasmon polariton antenna with dual-band endfire gain and flexible small frequency ratio," *IEEE Transactions on Antennas and Propagation*, Vol. 70, No. 11, 11 079–11 084, 2022.

[9] Imamvali, S., R. Chaparla, S. Tupakula, and D. Chaturvedi, "Novel SSPP sensor system with octagon-shaped unit cell for liquid analyte dielectric constant detection," in *2023 Photonics & Electromagnetics Research Symposium (PIERS)*, 1467–1473, Prague, Czech Republic, Jul. 2023.

[10] Imamvali, S., T. Nagarajan, R. Chaparala, and S. Tupakula, "Spoof surface plasmon polaritons based detection of glucose in blood phantom for medical diagnosis," *IEEE Sensors Journal*, Vol. 24, No. 23, 38 952–38 961, 2024.

[11] Kandwal, A., Q. Zhang, X.-L. Tang, L. W. Liu, and G. Zhang, "Low-profile spoof surface plasmon polaritons traveling-wave antenna for near-endfire radiation," *IEEE Antennas and Wireless Propagation Letters*, Vol. 17, No. 2, 184–187, 2018.

[12] Ge, S., Q. Zhang, A. K. Rashid, G. Zhang, C.-Y. Chiu, and R. D. Murch, "Analysis of asymmetrically corrugated goubau-line antenna for endfire radiation," *IEEE Transactions on Antennas and Propagation*, Vol. 67, No. 11, 7133–7138, 2019.

[13] Rudramuni, K., P. K. T. Rajanna, K. Kandaswamy, B. Majumder, and Q. Zhang, "Goubau line based end-fire antenna," *International Journal of RF and Microwave Computer-Aided Engineering*, Vol. 29, No. 12, e22008, 2019.

[14] O'Connor, E. M., D. R. Jackson, and S. A. Long, "Extension of the Hansen-Woodyard condition for endfire leaky-wave antennas," *IEEE Antennas and Wireless Propagation Letters*, Vol. 9, 1201–1204, 2010.

[15] Liu, L., M. Chen, and X. Yin, "Single-layer high gain endfire antenna based on spoof surface plasmon polaritons," *IEEE Access*, Vol. 8, 64 139–64 144, 2020.

[16] Ge, S., Q. Zhang, A. K. Rashid, H. Wang, and R. D. Murch, "Design of high-gain and small-aperture endfire antenna using a phase-reversal technique," *IEEE Transactions on Antennas and Propagation*, Vol. 68, No. 7, 5142–5150, 2020.

[17] Jiang, H., X.-Y. Cao, H.-H. Yang, J. Gao, and L.-R. Ji-Di, "Single-layer broadband endfire antenna with high-gain and stable beams based on spoof surface plasmon polaritons," *Radioengineering*, Vol. 31, No. 3, 295–301, 2022.

[18] Xiao, M., A. K. Rashid, B. Liu, R. Fan, and Q. Zhang, "Design of high-gain single-layer endfire antenna using phase-reversed asymmetric spoof surface plasmon polaritons," *IEEE Antennas and Wireless Propagation Letters*, Vol. 22, No. 3, 641–644, 2023.